Electrodeposition of biphasic calcium phosphate coatings with improved dissolution properties

Richard Drevet, Joël Fauré, Stephanie Sayen, Mélodie Marle-Spiess, Hassan El Btaouri, Hicham Benhayoune

Electrodeposition of biphasic calcium phosphate coatings with improved dissolution properties

Richard DREVET [1], Joël FAURE [2], Stéphanie SAYEN [3], Mélodie MARLE-SPIESS [2], Hassan EL BTAOURI [4] and Hicham BENHAYOUNE [2,*]

[1] CIRIMAT, Université de Toulouse, CNRS, INP- ENSIACET, 4 allée Emile Monso, BP44362, 31030 Toulouse cedex 4, France

[2] LISM EA 4695, Université de Reims Champagne-Ardenne, Bât. 6, Moulin de la Housse, BP 1039, 51687 Reims Cedex 2, France

[3] Institut de Chimie Moléculaire de Reims (ICMR), UMR CNRS 7312, Université de Reims Champagne-Ardenne, BP 1039, 51687 Reims Cedex 2, France

[4] UMR-CNRS 7369 Matrice Extracellulaire et Dynamique Cellulaire, UFR Sciences Exactes et Naturelles, Université de Reims Champagne Ardenne, Moulin de la Housse, BP 1039, 51687 Reims cedex, France

* Corresponding author

E-mail: hicham.benhayoune@univ-reims.fr

Tel.: +33 326 91 36 60

Abstract

Biphasic calcium phosphate coatings (hydroxyapatite/β-tricalcium phosphate) on titanium substrate (Ti6Al4V) are synthetized by pulsed current electrodeposition coupled to a thermal treatment under controlled atmosphere. The experimental conditions of the process such as the hydrogen peroxide amount and the treatment temperature are optimized in order to obtain different coatings compositions. The physico-chemical and structural characterizations of the coatings are carried out respectively by scanning electron microscopy associated with energy dispersive X-ray spectroscopy (SEM-EDXS) and X-ray diffraction (XRD). The *in vitro* dissolution-precipitation properties of the coated substrates are investigated by immersions into Dulbecco's Modified Eagle Medium (DMEM) from 1 to 28 days. The calcium and phosphorus concentrations variations in the biological liquid are assessed by Induced Coupled Plasma - Atomic Emission Spectroscopy (ICP-AES) for each immersion time. Furthermore, the corrosion behavior of the coated substrates are investigated using potentiodynamic polarization tests in DMEM and in Ringer's solution.

The results show that this innovative process is suitable to synthesize two coatings composed respectively of HAP (37%) / β-TCP (63%) and HAP (62%) / β-TCP (38%) with different morphologies. On the other hand, the *in vitro* studies reveal that the coatings composition greatly influences their behavior in physiological medium, i.e. their dissolution-precipitation and their corrosion protection properties.

Keywords: electrodeposition, biphasic coating, hydroxyapatite, β-tricalcium phosphate, dissolution-precipitation

1. Introduction

Nowadays, the bone implants used in orthopedics or dental surgeries are made of titanium alloys such as Ti6Al4V [1-2]. These alloys are particularly employed for their appropriate mechanical properties to replace the bone tissues and for their good biocompatibility with the body environment [3-4]. The bioactivity of their surface is commonly enhanced with calcium phosphate (CaP) coatings able to promote the bone growth onto the implant *in vivo* [5-6].

The bioactivity process starts with the partial dissolution of the calcium phosphate coating in contact with the physiological environment. The corresponding ionic releases induce an elevation of the local concentrations of the calcium and phosphate ions, leading to the precipitation of biological apatite on the surface of the implant. This behavior obviously depends on the solubility product (K_s) of the calcium phosphate material that defines the kinetics of these reactions when the biomaterial is implanted inside the body. Hydroxyapatite (HAP), the gold standard among the calcium phosphate materials is known to be highly stable [7-8]. This property is not much appropriate for coatings deposited on Ti6Al4V with the perspective to promote the biological activity of the bone implant. However, the solubility of the calcium phosphate coating can be enhanced by associating HAP with another calcium phosphate phase with higher solubility such as β-tricalcium phosphate (β-TCP). The dissolution behavior of the obtained biphasic coating is defined by the amount of each phase. Therefore, the biphasic calcium phosphate coatings have higher bioactivity and efficiency than those made of hydroxyapatite alone [9-10].

To produce calcium phosphate coatings onto implant surfaces, several methods can be used such as plasma spraying [11], RF-magnetron sputtering [12], pulsed laser-deposition [13], electrophoretic deposition [14], or electrodeposition [15-17]. This last one has many advantages upon the others since the thickness and the stoichiometry of the synthesized coatings can be controlled by the experimental conditions of the process [18]. However, the β-

TCP phase is only obtained at high temperatures (T > 800 °C), then a thermal treatment is required after electrodeposition to finalize the synthesis of the biphasic coating. To prevent the oxidation of the titanium alloy substrate, this thermal treatment has to be carried out under a controlled atmosphere, as described in the THUCA process developed in our recent works [19].

In that framework, the present research is describing for the first time to our knowledge, the electrodeposition of a biphasic calcium phosphate coating made of HAP and β-TCP. To assess the bioactivity of the coating, physicochemical characterizations are carried out before and after several immersion times in Dulbecco's Modified Eagle Medium (DMEM), a physiological solution that simulates the body fluids.

2. Material and Methods

2.1. HAP/β-TCP coatings electrodeposition

The CaP coatings were obtained by pulsed electrodeposition on Ti6Al4V substrates (discs of 12 mm in diameter and 4 mm in thickness). Before electrodeposition, the Ti6Al4V surfaces were blasted with alumina particles and etched in hydrofluoric acid for 8 seconds to produce an average roughness of 2 µm. Finally, they were ultrasonically cleaned in acetone and then in ultra-pure water. The electrolytic cell consists of a cathode (Ti6Al4V substrate), a counter electrode (Pt) and a reference saturated calomel electrode (SCE). The distance between the cathode and the counter electrode was 2 cm. The electrolyte was prepared by mixing a solution of 0.042 M $Ca(NO_3)_2{\cdot}4H_2O$ and 0.025 M $NH_4(H_2PO_4)$ without or with 9 vol.% of hydrogen peroxide (H_2O_2). The pH value was adjusted to 4.4 by adding 0.1 M NaOH solution and the temperature was fixed at 60 °C. The electrodeposition was performed with a potentiostat/galvanostat instrument (Voltalab PGP 201 Radiometer Analytical - VOLTAMASTER software) by pulsing the current [18]. A deposition time t_d = 1 min with a

current density j_d = 8 mA cm^{-2} was followed by a break time t_b = 2 min (j_b = 0 mA cm^{-2}). Seven pulse-cycles were used for a total deposition time of 21 minutes. Then, the electrodeposited CaP coatings were thermally treated under controlled atmosphere (argon flow) inside a tubular furnace (Nabertherm RS 80/500/11) according to the THUCA protocol developed in our laboratory [19]. A first plateau at 120 °C for 1 h to evaporate the solvents is followed by a second plateau at 1000 °C for 1 h. The controlled atmosphere is maintained until the complete cooling to room temperature. This thermal treatment totally crystallizes the phases of the coatings (HAP and β-TCP).

2.2. Scanning electron microscopy (SEM)

The surface morphologies of the CaP coatings were observed with a LaB_6 scanning electron microscope (JEOL JSM 6460 LV) operating at 0-30 kV. This microscope was associated with an energy dispersive X-ray spectrometer (EDXS) equipped with an ultra-thin Si(Li) window. The EDXS spectra were acquired for 100 s from a primary beam energy of 15 keV. The coating thickness was estimated by using a procedure previously developed in our laboratory for the calcium phosphate coating analysis [20].

2.3. X-ray diffraction (XRD)

X-ray diffraction (Bruker D8 Advance) was used to investigate the phases of the CaP coatings. The XRD patterns were collected from a monochromatic $Cu_{K\alpha}$ radiation for 2θ ranging from 20° to 50° with the step of 0.06° every 60 seconds. These experimental parameters were optimized to enhance the resolution for an accurate identification and quantification of the phases. The phases' identification was performed by using the Powder Diffraction Files (PDF) of the International Center for Diffraction Data (ICDD). The phases percentages and the Ca/P atomic ratio were calculated with the standard ISO 13779-3 for the

biphasic calcium phosphate materials [21]. This method consists in calculating the intensity ratio of the main peak for each phase and to compare its value to those of standard samples with known percentages.

2.4. Dissolution experiments

The experimental dissolution protocol is similar to the one developed in our previous works [22]. The samples are immersed in triplicate in 7 mL of Dulbecco's Modified Eagle Medium (DMEM). The chemical compositions of DMEM is given in **Table 1**. This physiological medium contains vitamins and amino acids for a composition close to that of the human blood plasma. The experiments were performed at 37 °C in a humidified atmosphere containing 5 vol.% of CO_2. Different incubation periods were tested: 1, 3, 7, 14, and 28 days. After each incubation period, the samples were retrieved, rinsed in distilled water and kept at 37 °C for SEM-EDXS and XRD analysis. Simultaneously, the physiological medium was collected to follow the Ca and P concentrations evolution using ICP-AES (Induced Coupled Plasma–Atomic Emission Spectroscopy, VARIAN Liberty Serie II). The measurements were performed in triplicate and the mean Ca and P concentrations were systematically compared to those of DMEM (reference) measured in the same experimental conditions.

2.5. *In vitro* electrochemical corrosion studies

The protective properties of the coatings were investigated using potentiodynamic polarization tests. The corrosion studies were performed in two different media: DMEM, used for ICP-AES analysis, and Ringer's solution (**Table 1**). This solution is typically used in research works about corrosion due to its saline composition and chemical aggressiveness. The potentiodynamic polarization curves were carried out by scanning the applied potential from -1.5 V vs SCE to + 1.5 V vs SCE with a scan rate of 10 mV s^{-1} using a

potentiostat/galvanostat instrument (Voltalab PGP 201 Radiometer Analytical - VOLTAMASTER software). Before the polarization, the samples reach the open circuit potential E_{OCP} for 15 min. Each test was repeated four times in order to reduce the margins of error and to verify the repeatability of the results. The temperature was maintained at 37 °C during the experiments. The extrapolation of the polarization curves provides the corrosion potential ($E_{corr.}$) and the corrosion current density ($i_{corr.}$).This last parameter is related to the corrosion rate (C_r) of the alloy that is calculated using the Faraday's law [23-26]:

$$C_r = \frac{i_{corr.} \times M}{n \times F \times \rho} \quad (1)$$

where M is the molar mass of Ti6Al4V (M = 446.1 g mol^{-1}), n is the number of transferred electrons during the corrosion reaction (estimated at n = 4 for Ti6Al4V), F is the Faraday constant (F = 96,500 C mol^{-1}), and ρ is the density of the alloy ($\rho_{Ti6Al4V}$ = 4.43 g cm^{-3}).

3. Results

The SEM micrographs of **Figure 1** show the morphology of the CaP coatings obtained without H_2O_2 (called CaP-0%) and with 9 vol.% H_2O_2 (called CaP-9%). The coating surface of CaP-0% is made of needles agglomerates and shows a low porosity (**Figure 1a**). The corresponding EDXS spectrum confirms that calcium and phosphorus are the main elements of the coating. Concurrently, **Figure 1b** presents the coating morphology of CaP-9%. One may clearly observe that the coating surface is made of spheroids with a low porosity similar to that observed for CaP-0%. The EDXS spectrum is similar to that of **Figure 1a**, indicating that the use of H_2O_2 does not affect the chemical composition of the coating. The estimated coating thickness is about 4.5 ± 0.3 µm in both cases. The XRD patterns of **Figure 2** show that both coatings are composed of two phases: hydroxyapatite (HAP) and β-tricalcium

phosphate (β-TCP). Indeed, the diffraction peaks observed at 2θ = 25.9°, 31.8°, 32.2°, 32.9°, 34.1° and 39.8° are the main ones of HAP (pdf # 09-0432). The diffraction peaks observed at 2θ = 27.8°, 31.1° and 34.4° are the main ones of the β-TCP phase (pdf # 09-0169). The calculated phase percentages are respectively 37% for HAP and 63% for β-TCP in the case of CaP-0% (**Figure 2a**), while the HAP percentage increases to 62% for CaP-9% (**Figure 2b**). From these results, the calculated Ca/P atomic ratio is respectively 1.55 and 1.60 for CaP-0% and CaP-9%. Moreover, the characteristic diffractions peaks are very thin for both specimens, indicating the high crystallinity of the coatings.

Next, the two coatings were immersed in DMEM from 1 to 28 days. In order to observe the evolution of the calcium and phosphorus concentrations in DMEM during the immersion tests, the Ca_{spec}/Ca_{DMEM} and P_{spec}/P_{DMEM} ratios were investigated by ICP-AES. The Ca_{spec} and P_{spec} are respectively the measured calcium and phosphorus concentrations in DMEM in contact with the coatings (specimen). The Ca_{DMEM} and P_{DMEM} are respectively the calcium and phosphorus concentrations in DMEM alone measured in the same experimental conditions (references). The obtained results are presented in **Figure 3**. The CaP-0% sample shows a significant increase of the two ratios after 1 day of immersion (**Figure 3a**). This result clearly reveals a high dissolution of the CaP coating in contact with DMEM. After 7 days of immersion, a significant decrease of the two ratios occurs and their values at 28 days are about 1, indicating that the precipitation reaction has started. For the CaP-9% sample, a significant increase of the two ratios is observed after 14 days which reveals that CaP-9% is more stable than CaP-0% and does not induce any significant precipitation at 28 days (**Figure 3b**). To illustrate these results, SEM-EDXS and XRD analysis were performed after 14 days of immersion. One may clearly observe a morphological change of the coatings surface, more pronounced in the case of CaP-0% (**Figure 4**). Indeed the needles observed before immersion disappeared and a spheroid-made morphology takes place (**Figure 4a**), while the

morphological change for CaP-9% only consists in the agglomeration of spheroids (**Figure 4b**). The corresponding EDXS spectra indicate that calcium and phosphorus are still the main elements of the coatings with the presence of some DMEM elements such as sodium and chlorine.

From the XRD analysis of **Figure 5**, the dissolution-precipitation process is highlighted by a strong decrease of the β-TCP diffraction peaks (2θ = 27.8°, 31.1° and 34.4°) associated to an increase of the HAP diffraction peaks (2θ = 25.9°, 31.8°, 32.2°, 32.9° and 34.1°). These phase changes are more pronounced in the case of the CaP-0% coating (**Figure 5a**) compared to the CaP-9% coating (**Figure 5b**).

On the other hand, one may observe a slight widening of the diffraction peaks in comparison with those of **Figure 2**, which suggests the decrease of the crystallinity of the coatings.

Furthermore, the corrosion behavior in DMEM of CaP-0% and CaP-9% was investigated by means of polarization curves. **Figure 6** shows the Tafel plots for the two samples compared to the uncoated Ti6Al4V substrate. A shift of the corrosion potential (E_{corr}) towards nobler values is visible for the coated Ti6Al4V samples. This shift is clearly more pronounced for the CaP-0% sample. The E_{corr} value increases from -0.923 V (uncoated Ti6Al4V) to -0.876 V (CaP-9%) and to -0.485 V (CaP-0%). Simultaneously the corrosion current (i_{corr}), i.e., the corrosion rate, strongly decreases as shown in **Table 2**. Thus, the two coatings act as protective barriers for the titanium substrate, improving the corrosion behavior in biological liquid. However, the CaP-0% coating is more protective than the CaP-9% coating, probably due to its higher reactivity with DMEM. To confirm this hypothesis, the corrosion behavior studies were repeated in Ringer's solution. The obtained results (**Figure 7** and **Table 3**) confirm that the corrosion protection is improved when the substrate is coated. The E_{corr} value increases from -0.935 V (uncoated Ti6Al4V) to -0.856 V (CaP-9%) and to -0.811V (CaP-0%). The E_{corr} values of the coated samples are similar since the Ringer's solution is an

aggressive and no-reactive medium. The decrease of the corrosion current is similar to that observed in DMEM.

4. Discussion

This research work describes an original protocol to synthesize a suitable calcium phosphate coating on a titanium alloy used for bone implants applications. The electrodeposited coating is made of two phases, hydroxyapatite characterized by a low bioactivity and β-tricalcium phosphate characterized by a high bioactivity [5-10].

The biphasic nature of the electrodeposited coating induces an appropriate bioactivity of the biomaterial the kinetics of which is tunable as a function of the amount of each phase. Indeed, the phases composition can be changed by the addition of hydrogen peroxide (H_2O_2) to the electrolyte solution used for the electrodeposition process [18].

The biphasic coating greatly improves the bioactivity of the prosthetic implant in comparison with that observed for a monophasic coating only made of stable hydroxyapatite [9,18].

The synthesis of the biphasic calcium phosphate coating occurs in two steps. First, the pulsed electrodeposition process induces the precipitation of an apatite layer according to reaction (2) [27]:

$$(10\text{-}x)\ Ca^{2+} + x\ HPO_4^{2-} + (6\text{-}x)\ PO_4^{3-} + (2\text{-}x)\ OH^- \rightarrow Ca_{10-x}(HPO_4)_x(PO_4)_{6-x}(OH)_{2-x} \quad (2)$$

with $0 < x < 1$

Then, the thermal treatment crystallized the apatite layer in two calcium phosphate phases according to reaction (3) [28]:

$$Ca_{10-x}(HPO_4)_x(PO_4)_{6-x}(OH)_{2-x} \rightarrow (1\text{-}x)\ Ca_{10}(PO_4)_6(OH)_2 + (x)\ 3Ca_3(PO_4)_2 + (x)\ H_2O \quad (3)$$

$$\text{apatite} \rightarrow (1\text{-}x)\ \text{HAP} + (x)\ 3\beta\text{-TCP} + (x)\ H_2O \quad \text{with } 0 < x < 1$$

The biphasic bulk or powder CaP materials made of HAP and β-TCP are widely described in literature for their high bioactivity in physiological environment.

Ebrahimi *et al.* indicate that the biphasic CaP have significant advantages over the other types of bioceramics by allowing a better control of bioactivity and biodegradation [29]. This behavior guarantees the stability of the biomaterial while promoting the bone ingrowth. The biphasic CaP are osteoconductive with the possibility of acquiring osteoinductive properties [30,31].

During the immersion in physiological medium, the calcium phosphates undergo a partial dissolution. The resulting local ionic supersaturation promotes the precipitation of a bone-like apatite able to create a continuous bond with the surrounding bone tissue [32]. This behavior defines the bioactivity of an implant material according to the definition proposed by Cao and Hench [33].

If the dissolution of the CaP material is too fast, the chemical interactions between the implant and the bone tissue do not take place adequately, resulting in anchorage failures to the bone [5].

That is the reason why the use of β-TCP alone is not appropriate whereas the biphasic calcium phosphates are a better choice for biomaterials applications [34].

According to the experimental conditions of our protocol, the amount of each calcium phosphate phase is tunable, providing a control of the kinetics of the chemical interactions inside the body. To study these chemical interactions, we have performed immersion experiments in a simulated body fluid, followed by morphological examinations of the surface

layer. The results show characteristic morphological changes induced by the dissolution-precipitation reactions occurring in the physiological solution. These reactions are more pronounced and more rapid for the CaP-0% sample in comparison with the CaP-9% sample. Moreover, the EDXS spectra of **Figure 4** obtained after immersion show the characteristic peaks of sodium and chlorine. This observation highlights that the new apatite layer includes some ions from the physiological medium to form a "bone-like" apatite [35].

This new layer presents appropriate chemical and morphological properties for the bone cells development. Indeed, Lee *et al.* have shown that the cell adhesion, spreading, proliferation, and differentiation is more active and more pronounced on the implant surfaces made of smooth elements [36].

More specifically, Cairns *et al.* have described the significant impact of a regular smooth topography on the osteocalcin expression and the alkaline phosphatase activity, promoting the bone cell growth in comparison with the rough surfaces made of needles [37].

At last, the corrosion studies show that the electrodeposited calcium phosphate coatings insulate and protect surface of the titanium alloy implant from the aggressive environment. The corrosion protection is essential to prevent the release of metal ions inside the body from the prosthetic implant, i.e. titanium, aluminum and vanadium ions [38]. The metal ions release is toxic for the patients, altering the expression of human lymphocyte-surface antigen and inhibiting the immune response assessed by lymphocyte proliferation [39,40]. The corrosion studies showed that the corrosion protection induced by the biphasic coating is associated to its reactivity in contact with the physiological medium.

Therefore, the new protocol developed in this research work produces a biphasic calcium phosphate coating with improved chemical and morphological properties for an optimized bioactivity in physiological environment.

5. Conclusion

In this work, biphasic calcium phosphate coatings (HAP/β-TCP) were prepared by pulsed electrodeposition current associated with a thermal treatment under controlled atmosphere. The physico-chemical and the structural analysis showed that the coatings composition and morphology depend on the H_2O_2 amount into the electrolytic solution. Indeed, with 9 vol.% H_2O_2, the phases percentage of the coating are 62% for HAP and 38% for β-TCP and its morphology is made of spheroids. However, without H_2O_2, these percentages are 37% for HAP and 63% for β-TCP with a morphology made of needles. The ICP-AES analysis revealed that the coating with the highest β-TCP percentage promotes the dissolution-precipitation processes and offers a better protection against corrosion of the metal alloy immersed in physiological medium.

6. References

[1] R. Boyer, G. Welsch, G. Collins, Materials Properties Handbook: Titanium Alloys, ASM international, Ohio, 1994.

[2] G. He, M. Hagiwara, Ti alloy design strategy for biomedical applications, Mater. Sci. Eng. C 26 (2006) 14-19.

[3] M. Geetha, A.K. Singh, R. Asokamani, A.K. Gogia, Ti based biomaterials, the ultimate choice for orthopaedic implants - A review, Progr. Mater. Sci. 54 (2009) 397-425.

[4] V. Sheremetyev, V. Brailovski, S. Prokoshkin, K. Inaekyan, S. Dubinskiy, Functional fatigue behavior of superelastic beta Ti-22Nb-6Zr(at%) alloy for load-bearing biomedical applications, Mater. Sci. Eng. C 58 (2016) 935-944.

[5] S.V. Dorozhkin, Bioceramics of calcium orthophosphates, Biomaterials 31 (2010) 1465-1485.

[6] S.R. Paital, N.B. Dahotre, Calcium phosphate coatings for bio-implant applications: Materials, performance factors, and methodologies, Mater. Sci. Eng. R 66 (2009) 1-70.

[7] R.Z. LeGeros, Calcium phosphate-based osteoinductive materials, Chem. Rev. 108 (2008) 4742-4753.

[8] M. Kohri, K. Miki, D.E. Waite, H. Nakajima, T. Okabe, In vitro stability of biphasic calcium phosphate ceramics, Biomaterials 14 (1993) 299-304.

[9] P. Ducheyne, S. Radin, L. King, The effect of calcium phosphate ceramic composition and structure on in vitro behavior. I. Dissolution, J. Biomed. Mater. Res. 27 (1993) 25-34.

[10] A. Seyfoori, Sh. Mirdamadi, Z.S. Seyedraoufi, A. Khavandi, M. Aliofkhazraei, Synthesis of biphasic calcium phosphate containing nanostructured films by micro arc oxidation on magnesium alloy, Mater. Chem. Phys. 142 (2013) 87-94.

[11] M. Chambard, O. Marsan, C. Charvillat, D. Grossin, P. Fort, C. Rey, F. Gitzhofer, G. Bertrand, Effect of the deposition route on the microstructure of plasma-sprayed hydroxyapatite coatings, Surf. Coat. Technol. 371 (2019) 68-77.

[12] D.Y. Lin, Y.T. Zhao, Preparation of novel hydroxyapatite/yttria-stabilized-zirconia gradient coatings by magnetron sputtering, Adv. Eng. Mater. 13 (2011) B18-B24.

[13] Y. Hashimoto, M. Kawashima, R. Hatanaka, M. Kusunoki, H. Nishikawa, S. Hontsu, M. Nakamura, Cytocompatibility of calcium phosphate coatings deposited by an ArF pulsed laser, J. Mater. Sci.: Mater. Med. 19 (2008) 327-333.

[14] R. Drevet, N. Ben Jaber, J. Fauré, A. Tara, A. Ben Cheikh Larbi, H. Benhayoune, Electrophoretic deposition (EPD) of nano-hydroxyapatite coatings with improved mechanical properties on prosthetic Ti6Al4V substrates, Surf. Coat. Technol. 301 (2016) 94-99.

[15] R. Drevet, Y. Zhukova, S. Dubinskiy, A. Kazakbiev, V. Naumenko, M. Abakumov, J. Fauré, H. Benhayoune, S. Prokoshkin, Electrodeposition of cobalt-substituted calcium phosphate coatings on Ti22Nb6Zr alloy for bone implant applications, J. Alloys Compd 793 (2019) 576-582.

[16] J.H. Park, Y.K. Lee, K.M. Kim, K.N. Kim, Bioactive calcium phosphate coating prepared on H_2O_2-treated titanium substrate by electrodeposition, Surf. Coat. Technol. 195 (2005) 252-257.

[17] R. Drevet, H. Benhayoune, L. Wortham, S. Potiron, J. Douglade, D. Laurent-Maquin, Effects of pulsed current and H_2O_2 amount on the composition of electrodeposited calcium phosphate coatings, Mater. Charact. 61 (2010) 786-795.

[18] H. Benhayoune, R. Drevet, J. Fauré , S. Potiron, T. Gloriant, H. Oudadesse, D. Laurent-Maquin, Elaboration of monophasic and biphasic calcium phosphate coatings on Ti6Al4V substrate by pulsed electrodeposition current, Adv. Eng. Mater. 12 (2010) B192-B199.

[19] N. Ben Jaber, R. Drevet, J. Fauré , C. Demangel, S. Potiron, A. Tara, A. Ben Cheikh Larbi, H. Benhayoune, A New Process for the Thermal Treatment of Calcium Phosphate Coatings Electrodeposited on Ti6Al4V Substrate, Adv. Eng. Mater. 17 (2015) 1608-1615.

[20] N. Dumelie, H. Benhayoune, G. Balossier, TF_Quantif: A procedure for quantitative mapping of thin films on heterogeneous substrates in electron probe microanalysis (EPMA), J. Phys. D:Appl. Phys. 40 (2007) 2124-2131.

[21] Implants for surgery - Hydroxyapatite - Part 3: Chemical analysis and characterization of crystallinity and phase purity, ISO 13779-3, 2008.

[22] R. Drevet, F. Velard, S. Potiron, D. Laurent-Maquin, H. Benhayoune, In vitro dissolution and corrosion study of calcium phosphate coatings elaborated by pulsed electrodeposition current on Ti6Al4V substrate, J. Mater. Sci.: Mater. Med. 22 (2011) 753-761.

[23] J. Tafel, Über die Polarisation bei kathodischer Wasserstoffentwicklung, Z. Phys. Chem. 50 (1905) 641-712.

[24] E. McCafferty, Validation of corrosion rates measured by the Tafel extrapolation method, Corros. Sci. 47 (2005) 3202-3215.

[25] R. Gene Ehl, A.J. Ihde, Faraday's electrochemical laws and the determination of equivalent weights, J. Chem. Educ. 31 (1954) 226-232.

[26] G.L. Turdean, A. Craciun, D. Popa, M. Constantiniuc, Study of electrochemical corrosion of biocompatible Co–Cr and Ni–Cr dental alloys in artificial saliva. Influence of pH of the solution, Mater. Chem. Phys. 233 (2019) 390-398.

[27] R.Z. Legeros, S. Lin, R. Rohanizadeh, D. Mijares, J.P. Legeros, Biphasic calcium phosphate bioceramics: Preparation, properties and applications, J. Mater. Sci.: Mater.Med. 14 (2003) 201-209.

[28] S.V. Dorozhkin, Biphasic, triphasic and multiphasic calcium orthophosphates, Acta Biomater. 8 (2012) 963-977.

[29] M. Ebrahimi, M.G. Botelho, S.V. Dorozhkin, Biphasic calcium phosphates bioceramics (HA/TCP): Concept, physicochemical properties and the impact of standardization of study protocols in biomaterials research, Mater. Sci. Eng. C 71 (2017) 1293-1312.

[30] G. Daculsi, R.Z. Legeros, E. Nery, K. Lynch, B. Kerebel, Transformation of biphasic calcium phosphate ceramics in vivo: ultrastructural and physicochemical characterization, J. Biomed. Mater. Res. 23 (1989) 883-894.

[31] G. Daculsi, R.Z. LeGeros, M. Heughebaert, I. Barbieux, Formation of carbonate-apatite crystals after implantation of calcium phosphate ceramics, Calcif. Tissue Int. 46 (1990) 20-27.

[32] N. Dumelie, H. Benhayoune, D. Richard, D. Laurent-Maquin, G. Balossier, In vitro precipitation of electrodeposited calcium-deficient hydroxyapatite coatings on Ti6Al4V substrate, Mater. Charact. 59 (2008) 129-133.

[33] W. Cao, L.L. Hench, Bioactive materials, Ceram. Int. 22 (1996) 493-507.

[34] S.V. Dorozhkin, Calcium orthophosphate deposits: Preparation, properties and biomedical applications, Mater. Sci. Eng. C 55 (2015) 272-326.

[35] H. Yang, K. Xia, T. Wang, J. Niu, Y. Song, Z. Xiong, K. Zheng, S. Wei, W. Lu, Growth, in vitro biodegradation and cytocompatibility properties of nano-hydroxyapatite coatings on biodegradable magnesium alloys, J. Alloys Compd. 672 (2016) 366-373.

[36] W.K. Lee, S.M. Lee, H.M. Kim, Effect of surface morphology of calcium phosphate on osteoblast-like HOS cell responses, J. Ind. Eng. Chem. 15 (2009) 677-682.

[37] M.L. Cairns, B.J. Meenan, G.A. Burke, A.R. Boyd, Influence of surface topography on osteoblast response to fibronectin coated calcium phosphate thin films, Colloids Surf. B Biointerfaces 78 (2010) 283-290.

[38] B.C. Costa, C.K. Tokuhara, L.A. Rocha, R.C. Oliveira, P.N. Lisboa-Filho, J.C. Pessoa, Vanadium ionic species from degradation of Ti-6Al-4V metallic implants: In vitro cytotoxicity and speciation evaluation, Mater. Sci. Eng. C 96 (2019) 730-739.

[39] E. Eisenbarth, D. Velten, M. Müller, R. Thull, J. Breme, Biocompatibility of β-stabilizing elements of titanium alloys, Biomaterials 25 (2004) 5705-5713.

[40] E. Eisenbarth, D. Velten, K. Schenk-Meuser, P. Linez, V. Biehl, H. Duschner, J. Breme, H. Hildebrand, Interactions between cells and titanium surfaces, Biomol. Eng. 19 (2002) 243-249.

Figure Captions

Fig. 1 SEM-EDXS characterizations of (a) the CaP-0% coating and (b) the CaP-9% coating.

Fig. 2 X-ray diffraction patterns of (a) the CaP-0% coating and (b) the CaP-9% coating.

Fig. 3 Calcium and phosphorus evolutions in DMEM as a function of the immersion time of (a) the CaP-0% coating and (b) the CaP-9% coating.

Fig. 4 SEM-EDXS characterizations after 14 days of immersion in DMEM of (a) the CaP-0% coating and (b) the CaP-9% coating.

Fig. 5 X-ray diffraction patterns after 14 days of immersion in DMEM of (a) the CaP-0% coating and (b) the CaP-9% coating.

Fig. 6 Polarization curves in DMEM of (a) the uncoated Ti6Al4V, (b) the CaP-0% coated Ti6Al4V and (c) the CaP-9% coated Ti6Al4V.

Fig. 7 Polarization curves in Ringer's solution of (a) the uncoated Ti6Al4V, (b) the CaP-0% coated Ti6Al4V and (c) the CaP-9% coated Ti6Al4V.

Fig.1

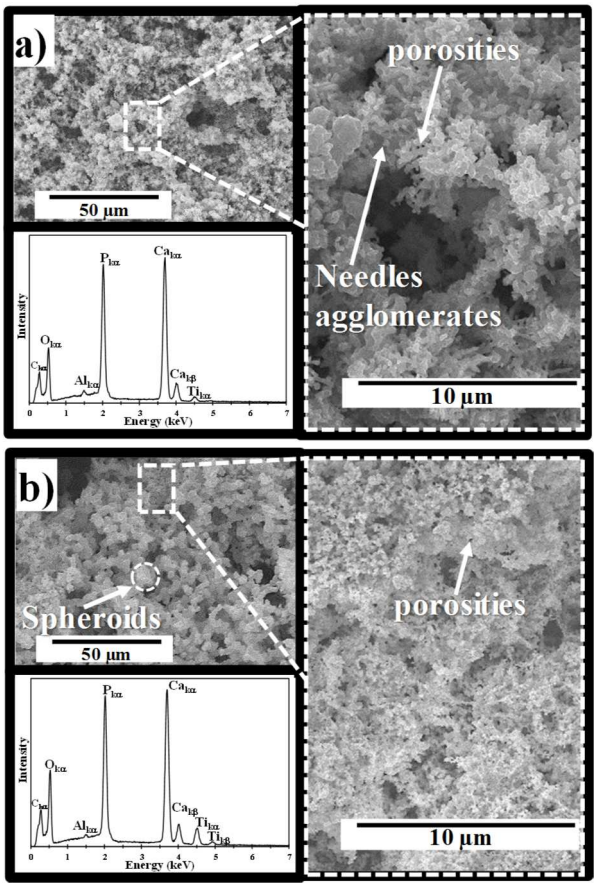
a)
50 µm
porosities
Needles
agglomerates
10 µm
Intensity
Energy (keV)
b)
Spheroids
50 µm
porosities
10 µm

Fig.2

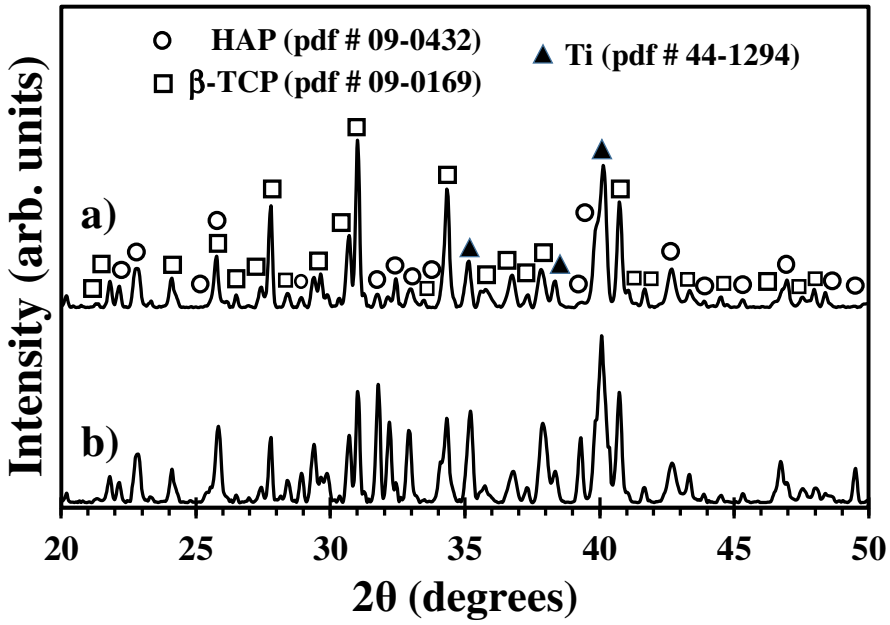
HAP (pdf # 09-0432)
β-TCP (pdf # 09-0169)
Ti (pdf # 44-1294)
a)
b)
Intensity (arb. units)
20
25
30
35
40
45
50
2θ (degrees)

Fig.3

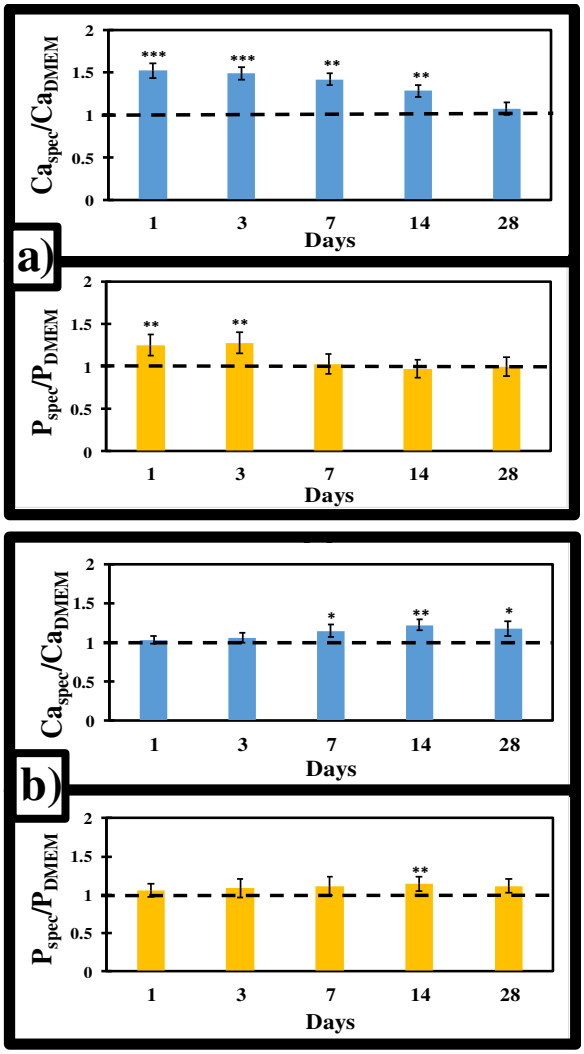
a)
Ca_{spec}/Ca_{DMEM}
P_{spec}/P_{DMEM}
b)
Ca_{spec}/Ca_{DMEM}
P_{spec}/P_{DMEM}
Days
0
0.5
1
1.5
2
1
3
7
14
28
*
**
***

Fig.4

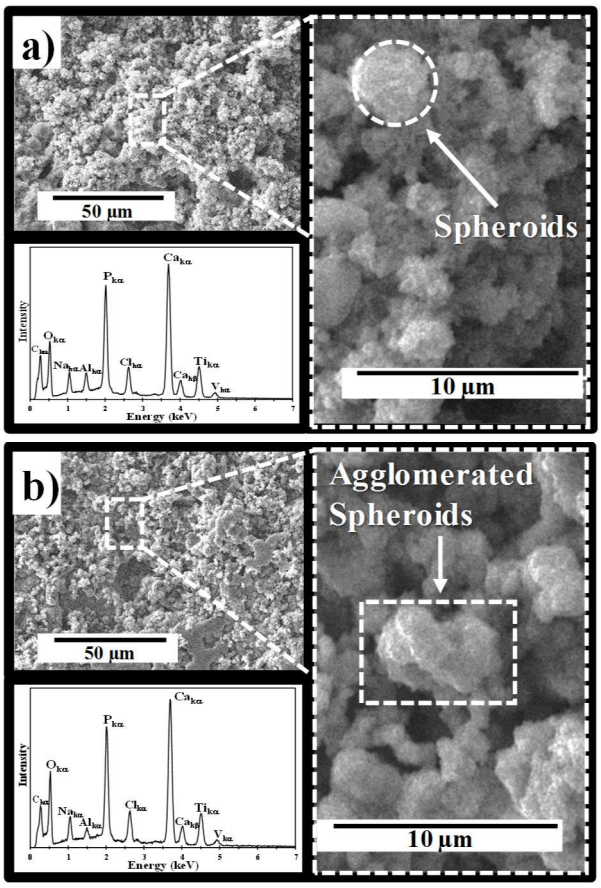
a)
50 µm
Spheroids
10 µm
Intensity
Energy (keV)
b)
50 µm
Agglomerated
Spheroids
10 µm
Intensity
Energy (keV)

Fig.5

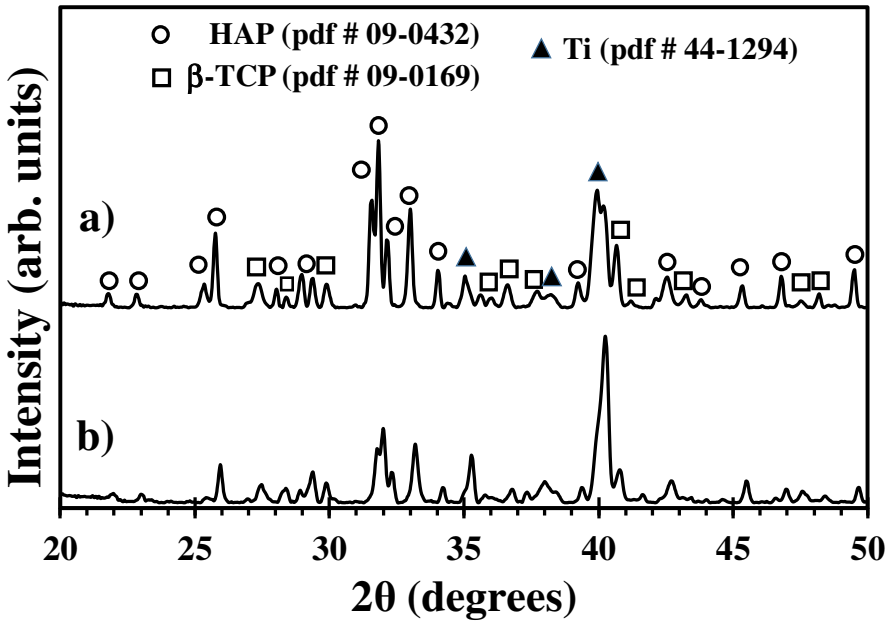
HAP (pdf # 09-0432)
β-TCP (pdf # 09-0169)
Ti (pdf # 44-1294)
a)
b)
Intensity (arb. units)
20
25
30
35
40
45
50
2θ (degrees)

Fig.6

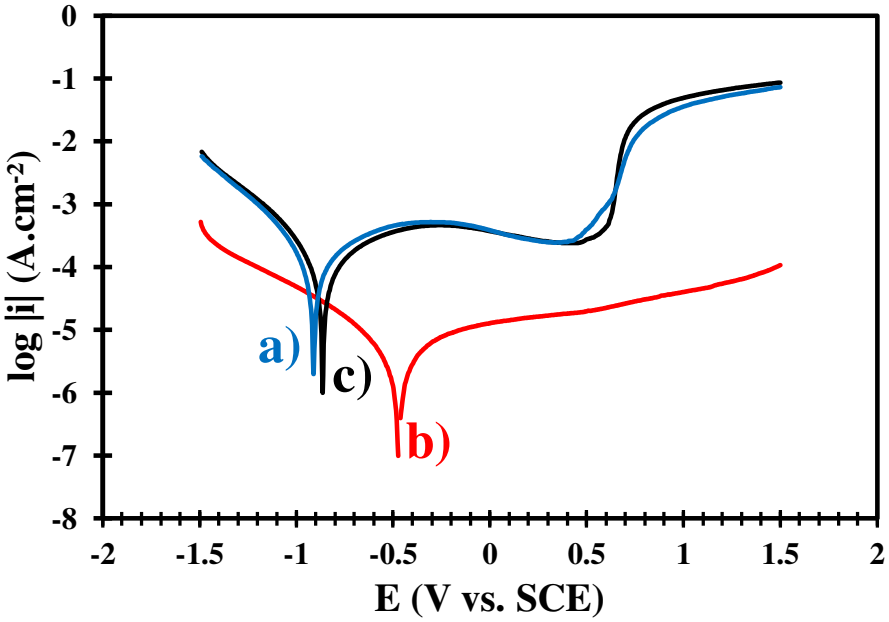

Fig.7

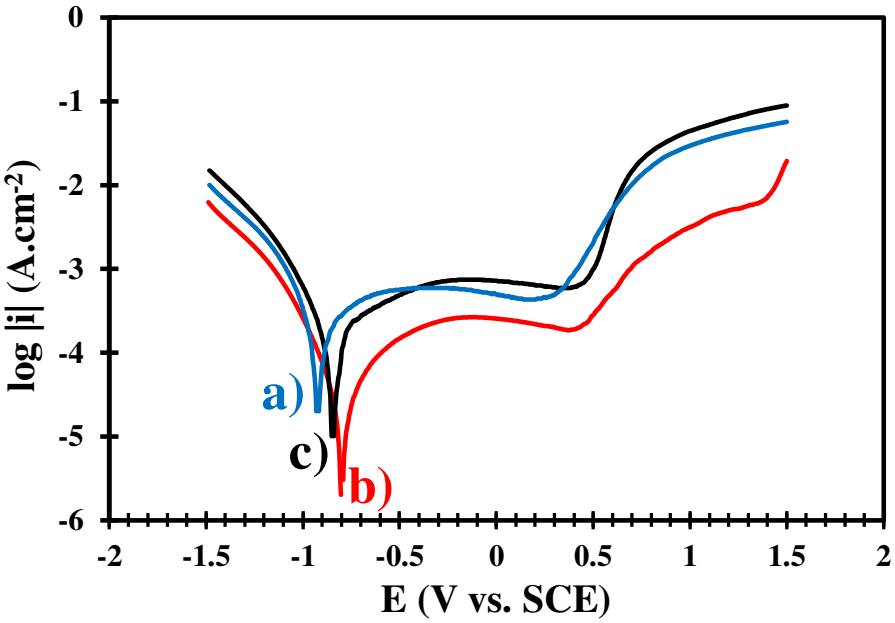

Table1: Chemical composition of the physiological solutions

Components	DMEM (g L^{-1})	Ringer (g L^{-1})
Inorganic salts		
NaCl	6.400	9.000
$NaHCO_3$	3.700	0.200
KCl	0.400	0.420
$CaCl_2$	0.264	0.480
$MgSO_4 \cdot 7H_2O$	0.200	-
$NaH_2PO_4 \cdot H_2O$	0.125	-
Other components		
Glucose	4.500	-
Sodium pyruvate	0.110	-
Phenol red Na	0.0159	-
Amino Acids		
L-Arginine·HCl	0.084	-
L-Cystine	0.048	-
L-Alanyl-L-glutamine	0.868	-
Glycine	0.030	-
L-Histidine HCl·H_2O	0.042	-
L-Isoleucine	0.105	-
L-Leucine	0.105	-
L-Lysine HCl	0.146	-
L-Methionine	0.030	-
L-Phenylalanine	0.066	-
L-Serine	0.042	-
L-Threonine	0.095	-
L-Tryptophan	0.016	-
L-Tyrosine	0.072	-
L-Valine	0.094	-
Vitamins		
D-calcium Pantothenate	0.004	-
Choline chloride	0.004	-
Folic acid	0.004	-
myo-Inositol	0.0072	-
Nicotinamide	0.004	-
Pyridoxine·HCl	0.004	-
Riboflavin	0.0004	-
Thiamine·HCl	0.004	-

Table2: corrosion parameters extracted from the polarization curves in DMEM

	$E_{corr.}$ (mV vs. SCE)	$i_{corr.}$ (µA cm^{-2})	C_r (mm yr^{-1})
CaP-0%	-485	1.1	0.01
CaP-9%	-876	32	0.26
Uncoated Ti6Al4V	-923	35	0.29

Table3: corrosion parameters extracted from the polarization curves in Ringer's solution

	$E_{corr.}$ (mV vs. SCE)	$i_{corr.}$ (µA cm^{-2})	C_r (mm yr^{-1})
CaP-0%	-811	12	0.10
CaP-9%	-856	56	0.46
Uncoated Ti6Al4V	-935	82	0.67